DOI: 10.1002/cssc.201000032

The Immobility of CO_2 in Marine Sediments Beneath 1500 Meters of Water

Kurt Zenz House,*[a] Bilgin Altundas,[b] Charlie F. Harvey,[a] and Daniel P. Schrag[c]

Injecting liquid CO_2 into deep-sea sediments below ca. 3 km of seawater has been suggested for the permanent storage of anthropogenic CO_2. At the pressures and temperature found below 3 km of seawater, CO_2 becomes denser than seawater and so is likely to remain permanently sequestered in the sediment. Deepwater engineering, however, is expensive and seawater depths of greater than 3 km are often only reached far from shore. Here, we consider the less expensive alternative of injecting CO_2 into marine sediments at depths shallower than required for denser-than-seawater CO_2 storage. We compare the mobility of liquid CO_2 that has been injected into deep-sea reservoirs with the mobility of supercritical CO_2 that has been injected into geologically equivalent (i.e., identical porosity, permeability, and effective stress) reservoirs with terrestrial pressure and temperature conditions. We demonstrate that buoyant liquid CO_2 with a density of about 90% that of seawater is sufficiently immobile that it can be considered trapped by gravity and capillarity. In contrast, supercritical CO_2 under typical terrestrial conditions is highly mobile and only trapped by the appropriate confining layer in either a structural or stratigraphic trap. As a result of its very high mobility under terrestrial conditions, CO_2 injected in an unconfined formation would spread beneath the confining layer to produce a large flat cylindrical-shaped plume of pure-phase CO_2. In contrast, the less mobile CO_2 in a typical deep-sea reservoir produces a spherical-shaped plume, resulting in a pure-phase-CO_2 footprint that is much smaller than the pure-phase-CO_2 footprint formed in the confined-terrestrial reservoir.

Introduction

The combustion of fossil fuels is likely to produce over 1000 GT of CO_2 from large point sources over the next 100 years without a dramatic shift in the means of global power production.[1,2] Technologies to capture CO_2 produced at industrial facilities and approaches to inject the CO_2 into geologic repositories are being pursued to help stabilize the concentration of atmospheric CO_2. When measured by pore-volume, there appears to be sufficient CO_2 capacity in terrestrial US basins to store thousands of years worth of current US emissions.[3–6] However, it may be difficult to guarantee the long-term confinement of buoyant CO_2 in terrestrial reservoirs that often contain fractures, faults, and abandoned wells and may be subject to pressure-induced fracturing.[7–9] Furthermore, securing the surface rights for injection can be expensive.

Storing CO_2 in deep-sea sediments has been proposed as an alternative to storing CO_2 in terrestrial formations.[10,11] Previous work has demonstrated that beneath ca. 2800 m of ocean, the pressure and temperature conditions compress CO_2 to a liquid phase that is denser than seawater.[11] Storing denser-than-seawater CO_2 in deep-sea sediments is inherently more secure then storing buoyant supercritical CO_2 in terrestrial formations because in the latter case, the CO_2 can escape through any conduit such as a fault or fracture.[9] The key benefit of deep-sea sediment storage is that confidence in the storage integrity derives from the known physical properties of CO_2 and seawater. In terrestrial reservoirs, on the other hand, CO_2 must be trapped by a confining layer of shale or clay.[12] As a result, ensuring the long-term storage of CO_2 in a terrestrial formation requires a detailed understanding of the structural geology; whereas ensuring such storage in appropriately deep marine sediments only requires knowledge of the in situ pressure and temperature.

Nearly 80% of the ocean floor within the 200 mile (1 mile = 1.609×10^3 m economic-free-zone of the US, however, is less than 3 km deep, and the sections of the ocean floor that are sufficiently deep tend to be >100 miles off the coast.[11] Construction of deep ocean pipelines costs ca. two million dollars per mile.[13] Bielicki has shown that there is nearly twice as much available storage area within the economic-free-zone at 2 km ocean depth as there is at 3 km ocean depth.[13] Therefore, storage of CO_2 in deep-sea sediments at depths shallower than 3 km would be both less expensive and more available, but it would not provide the storage assurance of negatively buoyant CO_2. As an alternative to storing denser-than-seawater CO_2 in sediments below ca. 3 km of seawater, we investigate the post-injection plume mobility of CO_2 stored in more shal-

[a] Dr. K. Z. House, Dr. C. F. Harvey
Department of Civil & Environmental Engineering
Massachusetts Institute of Technology (USA)
Fax: (+1) 617 258 6775
E-mail: khouse@mit.edu

[b] Dr. B. Altundas
Schlumberger Doll Research
1 Hampshire St., Cambridge, MA 02139-1578 (USA)

[c] Dr. D. P. Schrag
Department of Earth & Planetary Sciences
Harvard University (USA)

Supporting Information for this article is available on the WWW under http://dx.doi.org/10.1002/cssc.201000032.

low sediments. In these sediments, liquid CO_2 is between 5% and 10% less dense the seawater.

In this paper, we analyze long-term storage of *buoyant* liquid CO_2 injected into confined and unconfined deep-sea sediments. We compare the mobility of CO_2 in these marine sediments with the mobility in geologically equivalent terrestrial reservoirs with standard pressure and temperature (P&T) conditions. It is concluded that although the CO_2 is buoyant, as long as the P&T conditions are sufficient to yield liquid CO_2 with a density of about 90% that of seawater, then the CO_2 is sufficiently immobile that it can be considered trapped by gravity and capillarity. In contrast, the supercritical CO_2 injected into terrestrial reservoirs is highly mobile and only trapped under the appropriate geologic structures—such as structural or stratigraphic traps.

Physical Basis for Post-Injection CO_2 Mobility

Dimensional parameters

Three dimensionless parameters primarily govern the post-injection migration of CO_2 in porous media.[14] The first parameter is the buoyancy number:

$$\xi = \frac{\rho_{H_2O} - \rho_{CO_2}}{\rho_{H_2O}} \quad (1)$$

where ρ_{H_2O} is the density of the saline pore-fluid and ρ_{CO_2} is the density of CO_2. As the densities approach the same value, ξ approaches zero, and buoyancy-driven advection ceases. In addition, the vertical Darcy velocity scales linearly with ξ.[15] The second dimensionless parameter is the mobility number:

$$M = \frac{\mu_{H_2O}}{\mu_{CO_2}} \quad (2)$$

where μ_{H_2O} and μ_{CO_2} are, respectively, the viscosity of the saline pore water and the viscosity of the CO_2. M has been shown to dramatically affect the post-injection plume evolution.[16] In particular, the shape and the length of the gravity wave depend strongly on this ratio.[16] As M increases, the effect known as "gravity tonguing" increases, which results in thinner CO_2 plumes that occupy much greater reservoir areas.

The last key dimensionless parameter is the Bond number, which is the ratio of the buoyancy force to the capillary force:[14]

$$Bo = \frac{(\rho_{H_2O} - \rho_{CO_2})gr^2}{\gamma} \quad (3)$$

where g is the gravitational acceleration, r is the characteristic length scale of the curved surface interface, and γ is the interfacial surface tension between the CO_2 and the saline porewater. Because the CO_2/water interface is curved by the porous microstructure, the length scale (r) is the typical pore radius.[14]

H_2O is a more polar molecule than CO_2, and as a result, it has a greater affinity for the charged surfaces of rock than CO_2. With H_2O as the wetting phase and CO_2 as the nonwetting phase, the capillary force tends to resist migration, while the buoyancy force drives migration. Therefore, when Bo is $\gg 1$, buoyancy dominates and the CO_2 plume will tend to migrate significantly, while when Bo is $\ll 1$, then capillarity dominates and the plume will not migrate.

A larger ξ clearly leads to greater buoyancy driven advection, while decreases in M result in viscous fingering and further plume growth.[16] A small Bo indicates that capillary forces are strong relative to buoyancy forces, which results in greater capillary trapping of the CO_2. Therefore, conditions that result in smaller values of ξ, M, and Bo are better for long-term storage of CO_2.

Capillary breakthrough length

An alternative comparison between the buoyancy force and the capillary force can be made with the capillary breakthrough length (H). Specifically, the capillary breakthrough length estimates the quantity of buoyant fluid—CO_2 in this case—that can be trapped by the capillary pressure of the curved meniscus.[17] H is determined by balancing the buoyancy force and the capillary force:

$$F_B = \Delta\rho g H(\pi r^2) = F_C = \gamma(2\pi r)\cos(\theta) \quad (4)$$

where r is the pore-throat radius, H is the length of the fully connected pure-phase CO_2, and θ is the angle that the fluid meniscus makes with the pore-throat wall.[18] Thus, H is:

$$H = \frac{2\gamma\cos(\theta)}{\Delta\rho g r} \quad (5)$$

Table 1 compares the three key dimensionless parameters and the capillary breakthrough length for an 850 meter-deep terrestrial aquifer to the conditions typically found 800 meters below the seafloor and 2000 meters water depth.[19] It is notable that all three of the dimensionless parameters are substantially smaller—indicating less migration—in the deep-sea setting than in the terrestrial setting.

Table 1. Comparison of key dimensionless parameters and the capillary breakthrough length for a terrestrial aquifer to the conditions typically found 800 m below the seafloor with 2000 meters water depth.[a]

Reservoir	P [MPa]	T [K]	ξ	M	Bo	H
Terrestrial (Terr)	10	318	0.51	16.1	1.7×10^{-5}	1.2
Deep-sea (DS)	28	296	0.06	8.5	2.0×10^{-6}	10.0
Terr/DS ratio	NA	NA	9.2	1.9	8.6	0.1

[a] In both cases, a hydrostatic pressure gradient was assumed, while the geothermal gradients were taken to be 0.025 km^{-1}. The seafloor temperature was 276 K, while the terrestrial surface temperature was 293 K, and in both cases the pore-throat radii $= 10^{-5}$ m. The last row is the ratio of the value in the terrestrial setting to the value in the deep-sea setting.

The last row in Table 1 reveals the capillary breakthrough length in each setting. Here, θ is taken to be zero and r is taken to be ca. 10 μm for both the terrestrial and marine cases. In practice, r varies significantly, but in moderately permeable sandstone reservoirs is it typically on the order of 10 μm.[20] We choose to keep the wetting angle and the pore through equal in this analysis to elucidate the effects of the pressure and temperature.

It should be noted that H for a shale confining layer will be several orders of magnitude higher than for a reservoir layer due to its smaller pores. But, the differences in γ and $\Delta\rho$ between the two settings result in a capillary breakthrough length in the marine reservoir that is ca. 10 times larger than the value in the terrestrial reservoir. The larger H in the marine reservoir indicates that 10 times more pure-phase CO_2 must accumulate before the buoyancy force can overcome the capillary force.

All the physical parameters indicate that buoyant CO_2 injected into marine sediments will migrate less than CO_2 injected into hydrogeologically equivalent (i.e., equivalent porosity and permeability) terrestrial sediments. The ratios of these four parameters (Table 1) indicate that buoyant CO_2 injected beneath the seafloor will not migrate nearly as far as CO_2 that has been injected into a terrestrial reservoir.

Methods

Modeling of CO_2 plume migration

The pressure and temperature conditions differ dramatically between deep-sea sediments and terrestrial reservoirs. To study how these distinctly different conditions affect CO_2 plume migration, 3D reservoir simulations of CO_2 injection into four different reservoirs were performed with the commercial reservoir simulator ECLIPSE 300, and industry standard reservoir simulator for modeling multiphase flow in porous media with reactive transport. Comparative analysis between multiple reservoir simulators indicates strong agreement between the simulators regarding the behavior the stored CO_2.[21]

ECLIPSE 300 solves the multiphase flow equations for an input set of relative permeability curves and capillary pressure curves.[22] Most significantly, it simulates miscible flow by simultaneously solving the multiphase flow equations as well as the diffusion–advection equation for the miscible components. Solving the multiphase flow equations with dissolved transport is important for long-term simulations of geologic CO_2 storage. To elucidate the behavior of CO_2 under different pressure and temperature conditions, we performed simulations in four distinct reservoirs. We use the software to model the post-injection migration of CO_2 in a confined-terrestrial reservoir, an unconfined-terrestrial reservoir, a confined deep-sea reservoir, an unconfined deep-sea reservoir. The geologic properties of each class of reservoir (i.e., confined reservoirs and unconfined reservoirs) are identical. That is to say that the values of intrinsic vertical permeability (k_v), intrinsic horizontal permeability (k_h), and porosity (θ) are the same in the confined reservoirs under both P&T conditions. Likewise, those physical properties are the same in the unconfined reservoirs under both P&T conditions. In the unconfined reservoirs, the permeabilities are homogeneous and anisotropic: $k_v = 5\times10^{-15}$ m^2 and $k_h = 10^{-14}$ m^2. Whereas, in the confined reservoirs, the permeabilities are inhomogeneous and anisotropic with $k_v = k_h = 10^{-17}$ m^2 in the confining layer and $k_v = 5\times10^{-15}$ m^2 and $k_h = 10^{-14}$ m^2 in the reservoir layer. There are no tectonic forces in any of the simulations, and thus, the effective stresses (σ_{ij}) in all cases are the difference between the lithostatic pressure and the hydrostatic pressure. In addition, the reservoirs in all four simulations are not laterally confined. To accommodate that condition, the simulations were performed with sufficiently large reservoirs such that pressure in the outer most grid blocks were not affected by more than 1% during the injection.

Since the geologic properties are equivalent in each class of reservoir, the difference in CO_2 migration is due entirely to the different P&T conditions. For both the terrestrial reservoirs, the surface temperature and pressure are taken to be 288 K and 0.1 MPa, respectively, while the geothermal gradient is taken to be 0.025 K m.$^{-1}$ Therefore, the terrestrial conditions yield $\rho_{CO_2} \sim 560$ kg m^{-3} and $\mu_{CO_2} \sim 4\times10^{-5}$ kg m^{-1} s^{-1} at the well-screen. For both deep-sea reservoirs, the pressure at the bottom of the seafloor is taken to be 276 K, while the geothermal gradient is 0.03 km^{-1} Therefore, the deepsea conditions yield $\rho_{CO_2} \sim 930$ kg m^{-3} and $\mu_{CO_2} \sim 10^{-4}$ kg m^{-1} s^{-1} at the well-screen of our simulations.

The rate at which the CO_2 mobility parameters increase in the direction of greater mobility accelerates as the CO_2 critical point is approached and crossed.[19] Therefore, if the confining layer was below the critical point, then our simulations would overstate the mobility of CO_2 in confined terrestrial formations. Indeed, it is widely agreed upon in the CCS literature that terrestrial saline formations used for geologic storage of CO_2 should be at least ca. 800 m deep to ensure that the CO_2 remains in its supercritical state.[2] For that reason, the depth of the terrestrial simulations was selected such that the confining layer would be deeper than the point at which the static geologic conditions yield supercritical CO_2.

All four simulations involve the constant injection of 300 kT of CO_2 per year for 50 years per vertical injection well. The simulations are radially symmetric around the 100 m long vertical injection wells. In both confined cases, the confining layers ($k_v = k_h = 10^{-17}$ m^2) are 700 meters above the bottom of the well-screen. In the terrestrial unconfined case, CO_2 is injected into the reservoir from the bottom 100 meters of the aquifer, which is 1000 m thick, and 750 m to the surface from the wellhead. In that simulation, the CO2 migration is not modeled at depths shallower than 1100 m to avoid any phase changes near the surface. The accurate simulation of CO_2 during phase transitions is a critical area of ongoing research.[23]

Results

Confined terrestrial reservoir

The results of our simulations are partially shown in Figure 1. Figure 1a shows snapshots of the *confined-terrestrial* simula-

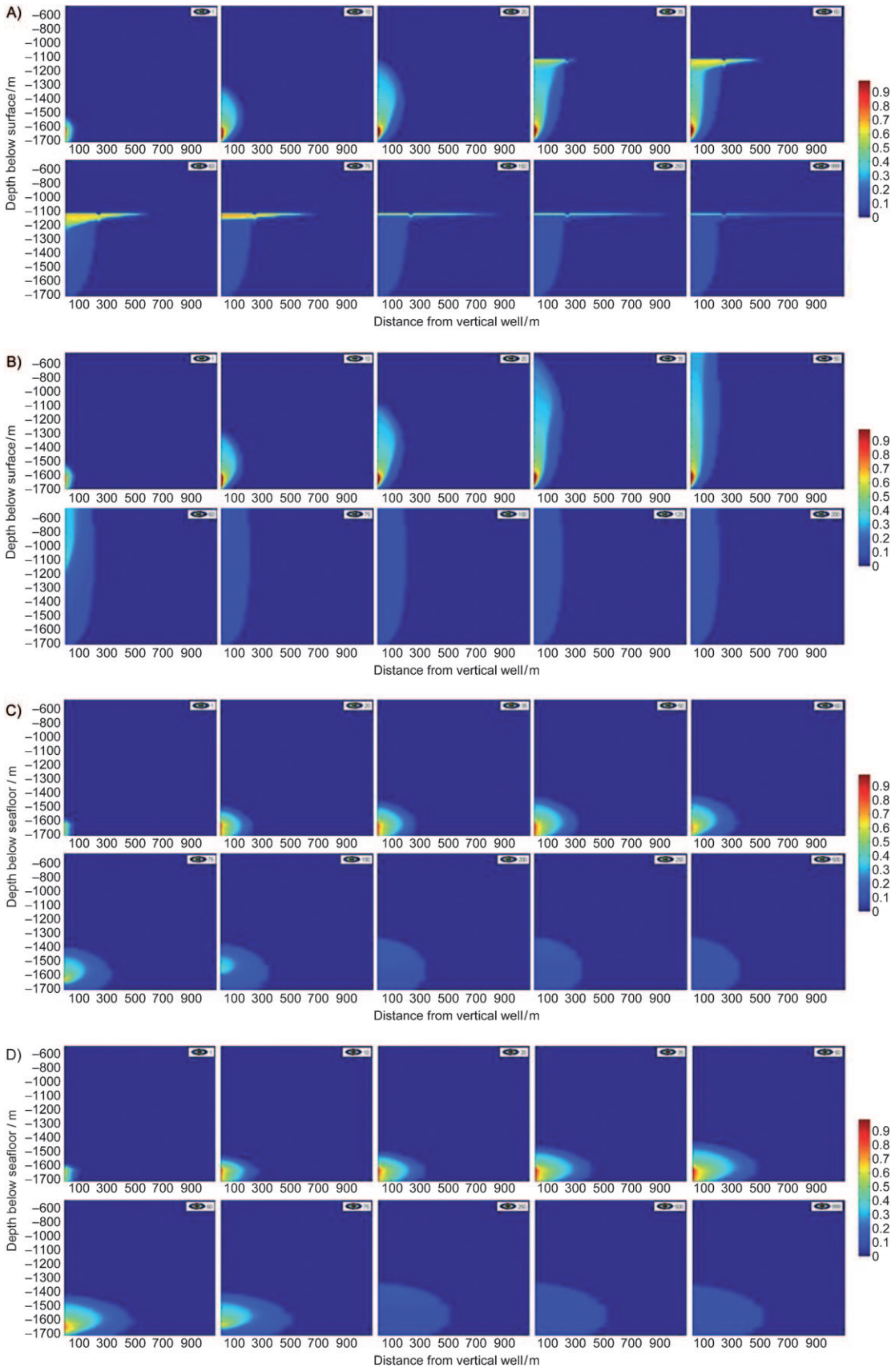

Figure 1. The injection and post-injection plume evolution for four simulations. In all cases, 300 kT of CO_2 is injected annually for 50 years. The physical properties of the reservoir (i.e., *kV*, k_h, porosity, and the effective stresses) are identical in all four simulations. A) Terrestrial P&T conditions with a confining layer ($k = 10^{-17}$ m^2 at 400 m below the top of the reservoir) 1000 meters below the surface. B) Terrestrial P&T conditions with no confining layer. C) P&T conditions of deep-sea sediments with no confining layer. D) P&T conditions of deep-sea sediments with a confining layer at 400 m below the seafloor.

tion. Specifically, the figure shows a vertical cross-section of the volumetric saturation field of pure-phase CO_2 [*S(x,r,z)*] during and after the injection, where each frame represents a slice through half of the radially symmetric plume. The 5th frame in the series shows *S(x,r,z)* at the end of the 50 year injection period. It is apparent from Figure 1a that on the injection time-scale, the pure-phase CO_2 migrates vertically to the bottom of the confining layer.

Figure 2a reveals the fraction of pure-phase CO_2 at each of the six 100 meter levels within the reservoir layer of the confined-terrestrial simulation. By the end of the 50 year injection period, about one-third of the pure-phase CO_2 resides in the top 100 meters of the reservoir. Once the injection ends, the accumulation of CO_2 beneath the confining layer accelerates as new CO_2 is not added to the deepest layer. The fraction of pure-phase CO_2 in that deepest layer starts decreasing immediately at the end of the injection, while the fraction of pure-phase CO_2 between 1500–1599 meters starts decreasing about two years after the end of the injection. The fraction of pure-phase CO_2 in the next three 100 meter levels between 1200 and 1499 meters below the surface starts to decline within 3, 6, and 8 years, respectively, after the end of the injection. Finally, the pure-phase CO_2 fraction in the top 100 meters peaks once that fraction in the other 5 levels is in decline.

After reaching its peak, the fraction of pure-phase CO_2 in the upper layer decreases because it dissolves more quickly than the pure-phase CO_2 in the lower levels. The variance in dissolution rates between depths is due to the greater horizontal advection at shallower depths. Ten years after the end of the injection, the horizontal extent of the pure-phase CO_2 in the upper 100 meters of the reservoir is 8 times longer than that of the pure-phase CO_2 in the deepest 100 meters. Since the simulations are radially symmetric, the CO_2 in the upper 100 meters encounters 64 times the volume of pore-water encountered by the lower levels. Therefore, the deeper pore-water becomes saturated with dissolved CO_2 more quickly than the shallower pore-water. As a result, at later times, pure-phase CO_2 dissolves more quickly in the shallow regions than in the deep regions.

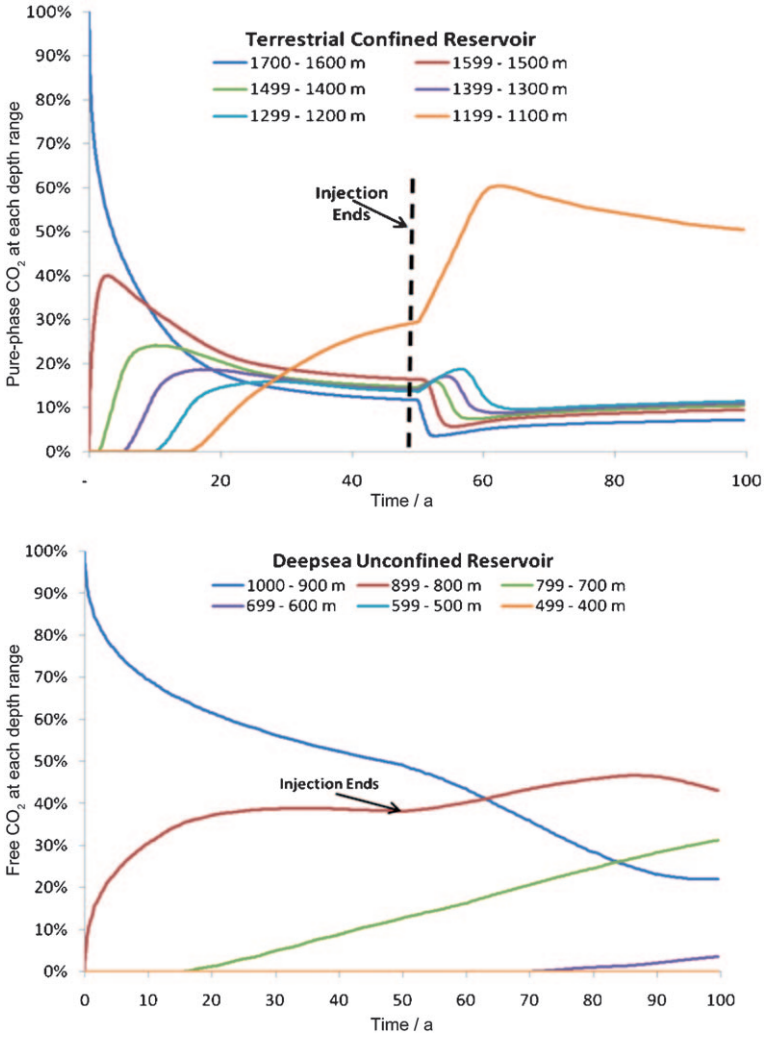

Figure 2. The fraction of free CO_2 at each of the six 100 meter depth levels within in the reservoir layer. A) Terrestrial confined reservoir: the upper 100 meters of the reservoir contains about one-third of the free CO_2 at the end of the injection period. B) Deep-sea confined reservoir: by the end of the injection, ca. 90% of the free CO_2 is in the deepest 200 meters of the reservoir.

The most important result of the confined-terrestrial simulations is the size of the free-gas CO_2 footprint. As can been seen in Figure 1a, the highly mobile CO_2 in the confined-terrestrial reservoir rapidly rises to the top of reservoir layer, and subsequently, it migrates laterally by buoyancy driven advection at the base of the confining layer. The aspect ratio of CO_2 plume increases dramatically as the CO_2 migrates horizontally resulting in a very long and very thin CO_2 plume. The modeling indicates that the pure-phase-CO_2 footprint for the confined-terrestrial case equals ca. 0.7 tonnes of CO_2) per m^2. Therefore, for a coal-fired power plant emitting 6 megatonnes of CO_2 per year, the CO_2 footprint for this confined-terrestrial homogeneous reservoir would be ca. 380 km^2. Such a large CO_2 footprint is concerning because the supercritical CO_2 is evidently highly mobile and will travel vertically through any conduit in the confining layer. The larger the CO_2 footprint, the harder it will be to confine the CO_2 because it will be difficult

to ensure that such a large subsurface region is free of faults, wells, and/or fractures.

Unconfined terrestrial reservoir

Figure 1b depicts snapshots of the *unconfined-terrestrial* simulation. The 5th frame in the series shows *S(x,r,z)* at the end of the 50 year injection period. It is apparent from Figure 1b that on the injection time scale, the pure-phase CO_2 migrates vertically through the reservoir and escapes to the atmosphere. That result is not surprising as the reservoir was unconfined, but it is striking how rapid and complete the CO_2 release is. Indeed, just 5 years after the end of the injection, a majority of the CO_2 had migrated into the zone shallower than 700 meters. In that depth range, the CO_2 transitions from the supercritical state to the vapor state resulting in a rapid increase in buoyancy and a rapid decrease in viscosity (Figure 3).

All the key mobility parameters accelerate sharply in the direction of greater mobility near the supercritical-vapor transition:

The rapid increase in CO_2 mobility at shallow depths in terrestrial formations (Table 2, Figure 3) indicates that CO_2 stored in terrestrial formations is unstable in the 650–900 m depth range. Thus, CO_2 escape from terrestrial formations can occur in accelerating form as depressurizing and cooling CO_2 becomes substantially more mobile.

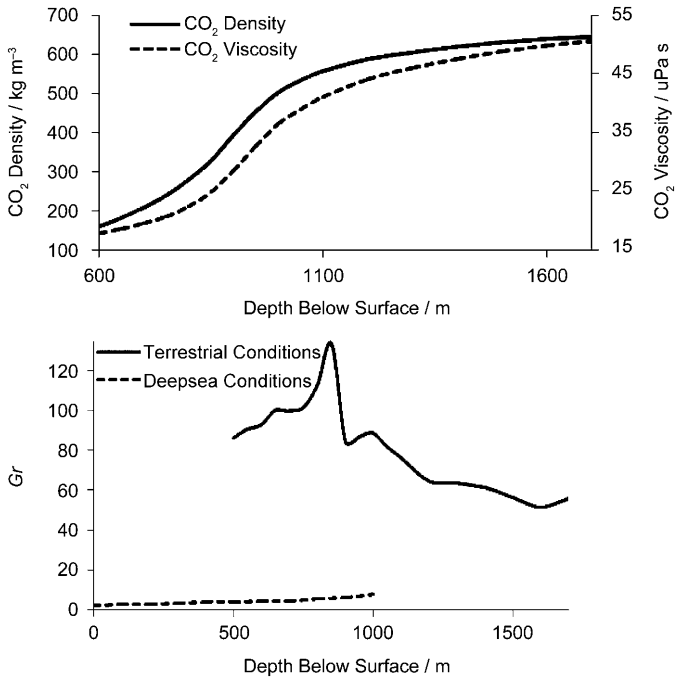

Figure 3. A) The density of CO_2 as a function of depth below the surface for typical terrestrial conditions. The surface temperature is taken to be 293 K, while the geothermal and pressure gradients are 0.025 km^{-1} and 0.01 $MPa\,m^{-1}$, respectively. It is evident from the figure that the compressibility of CO_2 increases sharply in the 700–950 m depth range that includes the transition from the vapor to the supercritical phase. In addition, the rate at which the viscosity increases with respect to the depth also increases in that depth range. B) The dimensionless parameter *Gr* is plotted against depth below the surface for both the terrestrial P&T conditions and deep-sea P&T conditions. In the latter case, the depth below surface is the depth below the seafloor. *Gr* determines the importance of the capillary force relative to the buoyancy force. The bigger *Gr* is, the less important the capillary force is.

Table 2. Key mobility parameters for a typical terrestrial formation at 650 meters deep (vapor) and 950 meters deep (supercritical).

CO_2	*P* [MPa]	*T* [K]	ξ	*M*	*Bo*	*H*
Vapor	6.5	309	0.82	38	2.2×10^{-5}	0.9
Supercritical	9.5	317	0.56	19	1.9×10^{-5}	1.0
Vapor/SC ratio	NA	NA	1.5	2.01	1.1	0.89

Unconfined deep-sea reservoir

Figure 1c depicts snapshots of the *unconfined deep-sea* simulation. Given that the porosity and permeability are the same in all 4 simulations, the difference between the unconfined terrestrial simulation and unconfined deep-sea simulation is dramatic. The 4th frame in the series shows *S(x,r,z)* at the end of the 50-year injection period. It is apparent from Figure 1c that—although the pure-phase CO_2 is 6% less dense than the pore-water—it barely migrates by buoyancy driven advection.

Figure 2b reveals the fraction of free CO_2 at each of the six 100 meter levels within the reservoir layer for the unconfined deep-sea simulation. By the end of the injection in the unconfined deep-sea reservoir, over 90% of the pure-phase CO_2 resides in the deepest 200 meters of the reservoir. In comparison, over half the pure-phase CO_2 in both terrestrial simulations had migrated more than 300 meters vertically. Similarly, two-thirds of the way through the injection, the time-averaged vertical front velocity of the CO_2 in the unconfined terrestrial simulation was ca. 26 $m\,a^{-1}$, while that metric in the unconfined deep-sea simulation was ca. 3.6 $m\,a^{-1}$.

The depletion rate for the pure-phase CO_2 fraction in the deepest layer decreases at the end of the injection, while the fraction of pure-phase CO_2 between 800–899 meters accelerates at the end of the injection. The fraction of pure-phase CO_2 between 700 and 799 meters below the seafloor increases at a steady rate over the next 50 years after the injection. The vast majority of the CO_2 never rises to depths shallower than ca. 700 meters. Indeed, 200 years after the end of the injection, 83% of the *buoyant* pure-phase CO_2 is still deeper than 700 meters below the seafloor. Over the subsequent 250 years (i.e., from 250 years after the end of the injection to 500 years after the end of the injection), the pure-phase CO_2 is essentially immobile as the fractions of CO_2 residing in the each of the 3 deepest 100 meter levels changes by less than 1% each. Likewise, after 950 years of post-injection evolution, 88% of the pure-phase CO_2 resides in the deepest 200 meters. The increase in the pure-phase fraction between 450 and 950 years after the end of the injection is primarily due to the higher CO_2 dissolution rates at shallow depths as the pure-phase CO_2 mixes with greater volumes of pore-water the farther it migrates.

An important comparison can be made between the pure-phase-CO_2 footprint of the confined terrestrial simulation and

the unconfined deep-sea simulation. As can be seen in Figure 1a, the highly mobile CO_2 in the confined terrestrial reservoir rapidly migrates laterally by buoyancy driven advection at the base of the confining layer. In contrast, the highly immobile CO_2 in the unconfined deep-sea reservoir essentially forms a sphere of pure-phase CO_2 around the well-screen (Figure 1c). While the aspect ratio of the confined terrestrial case grows rapidly in the post-injection period, it is nearly unity in the deep-sea unconfined case for 1000 years. The modeling indicates that the pure-phase-CO2 footprint for the unconfined deep-sea case equals ca. 35 tonnes of CO_2 per m^2 of seafloor. That compares to ca. 0.7 tonnes of CO_2 per m^2 of terrestrial land surface. Therefore, the deep-sea sediments can store ca. 50 times more mass of CO_2 per unit area than a typical terrestrial formation.

For a coal-fired power plant emitting 6 MT of CO_2 per year, the pure-phase-CO_2 footprint for an unconfined deep-sea reservoir would be ca. 8 km^2 compared to 380 km^2 in the confined terrestrial case. Such a small footprint is beneficial for several reasons. Furthermore, the risk of CO_2 escape is diminished by a smaller footprint as it is easier to fully characterize the subsurface conditions for a small footprint than for a large footprint.

Confined deep-sea reservoir

For completeness, the same simulations were performed for a confined deep-sea reservoir with the confining layer 600 meters above the bottom of the well-screen as in the confined terrestrial case. As was demonstrated by the unconfined deep-sea simulations, CO_2 at deep-sea P&T conditions is highly immobile. The results of the confined deep-sea simulations (Figure 1d) are almost identical to those for the unconfined deep-sea case. That is not surprising because the pure-phase CO_2 did not migrate more than ca. 300 meters vertically in the unconfined deep-sea case. Thus, all the results described in the unconfined deep-sea case apply to the confined deep-sea case.

Discussion

In the Supporting Information we derive a one-dimensional model to explain the differing behaviors of the terrestrial and submarine plumes. This model elucidates the importance of the mobility parameters so that we can consider how the simulation results depend of the parameter values. The 1D model is formulated to relate the change in CO_2 saturation to the vertical divergence of pressure:

$$\frac{\partial S}{\partial \hat{T}} = \frac{\partial}{\partial \hat{Z}}\left[k_{rc}(1-f_c) - k_{rc}(1-f_c)\frac{1}{Gr}\frac{dJ(S)}{d\hat{Z}}\right] \quad (6)$$

where,

$$Gr = \frac{\Delta\rho g L_z \sqrt{k/\phi}}{\sigma} \quad (7)$$

As Gr decreases, the relative the importance of capillary force relative to both the gravitational and viscous forces grows. The primary variables that compose Gr are the surface tension (σ), the density difference ($\Delta\rho$), the depth of the injection (L_z), the intrinsic permeability (k), and the porosity (ϕ).

The larger Gr, the less important the capillary force is relative to the buoyancy force. Figure 3b reveals the value of Gr as a function of depth below the surface for both terrestrial and deep-sea P&T conditions. In the latter case, the depth below the surface is the depth below the seafloor. The values of Gr in Figure 3b were calculated with homogenous and isotropic permeability ($k = 10^{-14}$ m^2) and porosity ($\phi = 0.15$) values, so the change in Gr with depth depends on $\Delta\rho$ and σ.[24]

It is apparent from Figure 3b that Gr under typical terrestrial condition is between about 10 and 50 times bigger than Gr under typical marine conditions, which indicates that the capillary force is much more important relative to the buoyancy force in a deep-sea reservoir than in a terrestrial reservoir. Furthermore, the absolute values shown in Figure 3b indicate that under typical terrestrial conditions $1/Gr$ is on the order of 10^{-2}, and thus, the capillary term in Equation (6) can be dropped for most capillary pressure functions. Indeed, other analytic models of post-injection CO_2-plume evolution in terrestrial reservoirs ignore capillary effects.[25]

Under typical deep-sea conditions, on the other hand, $1/Gr$ is on the order of 0.1–1.0. Therefore, in deep-sea reservoirs, the capillary force and the buoyancy force affect the CO_2 plume migration to a similar degree. Since the pore-water is the wetting phase,[26] then the capillary force tends to draw water into the CO_2 plume, which tends to resist buoyancy-driven migration. The result of this near-balance between buoyancy and gravity is evident in Figure 1c and d. In both of those simulations, buoyant CO_2—with a density of about 94% that of the pore-water—is essentially immobile for 950 years after the injection is complete.

Conclusion

Nearly 34 billion tonnes of CO_2 was produced globally in 2007.[1] We believe that stabilizing atmospheric CO_2 within this century will require the storage of approximately 1000 GT of CO_2 over the next 100 years. We have demonstrated that supercritical CO_2 injected into typical terrestrial reservoirs is highly mobile, and its mobility can result in a pure-phase CO_2 footprint of ~0.7 tonnes of CO_2 per square meter. In comparison, liquid CO_2 in deepsea sediments is highly immobile, and its immobility will result in a pure-phase-CO_2 footprint of ca. 35 tonnes per square meter. The factor of ca. 50 between the two footprints is significant. If 1000 GT of CO_2 were injected into typical terrestrial reservoirs over the next 100 years, then those reservoirs would comprise a footprint of approximately 1.4 million km^2; whereas, if that mass of CO_2 were injected into typical deepsea sediments, then the total CO_2 footprint would equal about 29 000 km^2. The much smaller footprint combined with the dramatically lower mobility of liquid CO_2 in deepsea sediments suggests that storage of CO_2 in deep-sea sediments could play a large role in CO_2 emissions abatement.

Keywords: carbon storage · industrial chemistry · molecular modeling · physical chemistry · supercritical fluids

[1] M. R. Raupach, G. Marland, P. Ciais, C. Le Quere, J. G. Canadell, G. Klepper, C. B. Field, *Proc. Natl. Acad. Sci. USA* **2007**, *104*, 10288 – 10293.
[2] E. Rubin, L. Meyer et al., in *IPCC Special Report on Carbon Dioxide Capture and Storage. Prepared by Working Group III of the Intergovernmental Panel on Climate Change*, Intergovernmental Panel on Climate Change, Cambridge **2005**.
[3] *The Midwest Regional Carbon Sequestration Partnership*, Battelle Memorial Institute and US Department of Energy, **2005**.
[4] R. Finely et. al. , in *An Assessment of Geological Carbon Sequestration Options in the Illinois Basin*, Midwest Geological Sequestration Consortium and US Department of Energy, **2005**.
[5] L. Myer, C. Downey et al., in *An Overview of Geologic Carbon Sequestration Potential in California*, US Department of Energy, **2005**.
[6] B. McPherson et. al., *Southwest Regional Partnership on Carbon Sequestration*, New Mexico Institute of Mining of Technology and U. S. Department of Energy, **2006**.
[7] Z. K. Shipton, J. P. Evans et al., *Geol. Soc. Spec. Publ.* **2004**, *233*, 43 – 58.
[8] J. Nordbotten, M. Celia, S. Bachu, H. K. Dahle, *Environ. Sci. Technol.* **2005**, *39*, 602 – 611.
[9] C. M. Oldenburg, J. L. Lewicki, *Environm. Geol.* **2005**, *50*, 691 – 705.
[10] H. E. A. Koide, *Energy Convers. Manage.* **1997**, *38*, 253 – 258.
[11] K. Z. House, D. Schrag, C. F. Harvey, K. S. Lackner, *Proc. Natl. Acad. Sci. USA* **2006**, *103*, 12291 – 12295.
[12] S. Benson, P. Cook, *Underground Geology Storage*, in *IPCC Special Report on Carbon Dioxide Capture and Storage*, Intergovernmental Panel on Climate Change, Cambridge, **2005**.
[13] J. Bielicki, *The Viability of Permanent Carbon Capture and Storage in Deep Sea Sediment*, AGU Fall Meeting, San Francisco, **2007**.
[14] V. Frette, J. Feder, T. Jossang, P. Meakin, *Phys. Rev. Lett.* **1992**, *68*, 3164 – 3167.
[15] P. A. F. Domenico, W. Schwarts, *Physical and Chemical Hydrogeology*, John Wiley & Sons, New York, **1998**.
[16] R. Juanes, C. W. MacMinn, *Soc. Pet. Eng.* **2008**, 113496.
[17] B. V. Zhmud, F. Tiberg, K. Hallstensson, *J. Colloid Interface Sci.* **2000**, *228*, 263 – 269.
[18] P.-G. de Gennes, F. Brochard-Wyart et al., in *Capillary and Wetting Phenomena*, Springer, New York, **2003**.
[19] E. W. Lemmon, M. O. McLinden, *Thermophysical Properties of Fluid Systems*, in *NIST Chemistry WebBook*, National Institute of Standards and Technology, Gaithersburg, **2005**.
[20] H. Pape, J. E. Tillich, M. Holz, *J. Appl. Geophys.* **2006**, *58*, 232 – 252.
[21] K. Pruess, J. Garcia, T. Kovscek, C. Oldenburg, J. Rutqvist, C. Steefel, T. F. Xu, *Energy* **2004**, *29*, 1431 – 1444.
[22] *ECLIPSE Reference Manual*, Schlumberger, Inc, **2007**.
[23] K. Pruess, *Numerical simulation of CO_2 leakage from a geologic disposal reservoir including transitions from super- to subcritical conditions, and boiling of liquid of CO_2*, Lawrence Berkeley National Laboratory, **2003**.
[24] B.-S. Chun, G. Wilkinson, *Ind. Eng. Chem. Res.* **1995**, *34*, 4371 – 4377.
[25] S. Lyle, H. Huppert, M. Hallworth, M. Bickle, A. Chadwick, *J. Fluid Mech.* **2005**, *543*, 293 – 302.
[26] K. Pruess, C. Doughty, *Vadose Zone J.* **2004**, *3*, 738 – 746.

Received: February 10, 2010
Published online on August 4, 2010

